Supporting Information

Label-Free Biochemical Analytic Method for the Early Detection of Adenoviral Conjunctivitis Using Human Tear Biofluids

Samjin Choi[1,2,3,*], Sung Woon Moon[4], Jae-Ho Shin[4], Hun-Kuk Park[1,2,3] and Kyung-Hyun Jin[4,*]

1. Department of Biomedical Engineering, College of Medicine, Kyung Hee University, Seoul 130-701, Korea

2. Healthcare Industry Research Institute, Kyung Hee University, Seoul 130-701, Korea

3. Department of Medical Engineering, College of Medicine, Kyung Hee University, Seoul 130-701, Korea

4. Department of Ophthalmology, Kyung Hee University, Seoul 130-701, Korea

*Correspondence should be addressed to K.H. Jin and S. Choi (medchoi@khu.ac.kr).

We added a total of nineteen supporting documents consisting of nine figures and ten tables.

Target journals: Analytical Chemistry

■ Previous report of tear fluid analysis

Table S1. Summary of tear fluidic proteomic studies using drop-coating deposition surface-enhanced Raman scattering (DCD-SERS).

Reference	Tear volume (μL)	Surface enhanced material	Tear collection	Disease	Year
Zhang et al.[1]	2 (1–10)	Au and Teflon	Synthetic tear	-	2003
Reyes-Goddard et al.[2]	0.5	Au and Ag	Synthetic tear	Herpes simplex virus	2008
Filik and Stone[3]	1 and 1.5	CaF_2	Capillary tube	-	2008
Filik and Stone[4]	1.5	CaF_2	Synthetic tear	-	2007
Kuo et al.[5]	1.5	Ti/Au	Microcapillary tube	Infectious (*Pseudomonas aeruginosa* and *Streptococcus pneumonia*) and noninfectious ulcerative keratitis	2011
Kuo et al.[6]	1.5	Ti/Au	Microcapillary tube	Infectious and noninfectious ulcerative keratitis	2012
This study	2	Au	Microfilter	Adenoviral conjunctivitis	2014

■ Principal component analysis

In general, the principal component analysis (PCA) is used to enhance representation of data and reduce dimensionality. PCA is applied to data that contains correlated dependent variables. PCA allows for the extraction of the important information from data and it is represented as a set of new orthogonal variables called principal components (PCs). The pattern of similarity of the observations and of the variables can then be mapped.[7] The PC P_1 of dataset X can be defined as

$$P_1 = arg\ \max_{\|P\|=1} var\left\{P^T X\right\} = arg\ \max_{\|P\|=1} E\left\{\left(P^T X\right)^2\right\}. \quad \text{(S1)}$$

Herein, the m-th component is deduced by subtracting the first $m-1$ PCs from X to yield

$$\hat{X}_{m-1} = X - \sum_{i=1}^{m-1} P_i P_i^T X\ , \quad \text{(S2)}$$

and this result is used as a new entry to find a PC. X is the projected down into reduced space defined by only the first n singular vectors (P_n), where $Y=P_n^T X$.

■ Gaussian function

Let $g_k(f)$ represent the discrete version of a Gaussian function, defined as

$$g_k(f) = H_k \cdot \exp\left(\frac{(f - f_k)^2}{2w_k^{\,2}}\right), \tag{S3}$$

where H_k denotes the amplitude of a Gaussian peak, f_k denotes the maximum frequency position of a Gaussian peak, and w_k denotes the half-width of a Gaussian peak. The fitted spectral Gaussian curve can be represented by a sum of each Gaussian function as follows,

$$G(f) = \sum_{k=1}^{m} g_k(f), \tag{S4}$$

where m denotes the number of total Gaussian functions.[8,9]

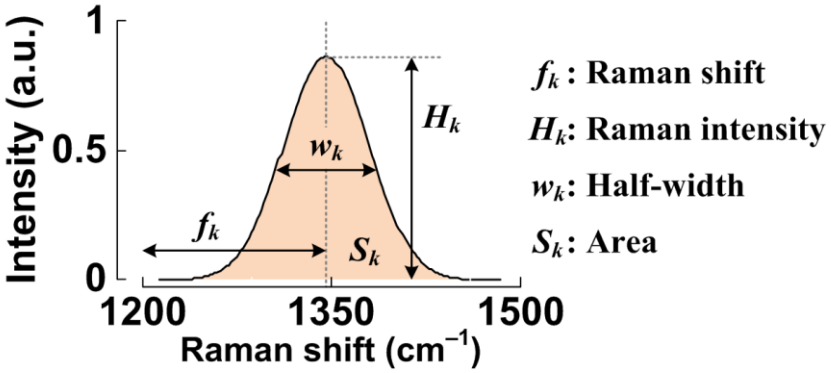

Figure S1. Spectral parameters for evaluating a single Gaussian function.

■ Characterization of DCD-SERS methodology

All DCD-SERS spectra in this study were measured using a self-made 50-nm thick Au-coated nanodot array substrate.[10] This low-cost AAO nanoplasmonic Au nanodot array substrate was verified by comparing it with an equal-thickness commercial SERS substrate (Au.0500.ALSI, Platypus Technologies). The surface morphology of the two SERS substrates was characterized using a tapping-mode AFM machine (NANOS N8 NEOS, Bruker, Herzogenrath, Germany). Both substrates showed uniform surface structure (Figure S2), and the 50-nm Au/2.5-nm Ti Platypus® gold substrate had a ten-fold decrease in surface roughness compared to the nanoplasmonic gold nanodot array substrate (Table S2). Additionally, SERS activity of two substrates was investigated using 2 μL of balanced salt solution (BSS; pH 7.5, 300 mOsm/kg), an isotonic solution used clinically to irrigate tissues of the eyes (Figure S3). The seven prominent Raman bands at 839 cm^{-1} (symmetric C–C–C stretching vibration of the proline ring), 945 and 969 cm^{-1} (symmetric C–C stretching vibration of the acetate anion), 1060–1078 cm^{-1} (symmetric C–N stretching vibration), 1356 cm^{-1} (symmetric bending vibration of the methyl CH_3 group), and 1438 and 1462 cm^{-1} (antisymmetric deformation of the methyl CH_3 group or symmetric deformation of the methylene CH_2 group) were assigned according to the literature.[11,12] Both SERS substrates produced similar spectral patterns. However, the AAO nanoplasmonic gold nanodot

array substrate produced approximately two-fold stronger intensities when compared to the Au.0500.ALSI substrate. Overall, the nanoplasmonic gold nanodot array substrate showed superior nanostructure and activity for use in DCD-SERS spectra measurement than the commercial SERS substrate Au.0500.ALSI.

In order to reduce variation in DCD-SERS spectral intensity, all DCD-SERS spectral signals were pre-processed with baseline-correction and normalization. Representative DCD-SERS spectra of the normal and adenovirus-infected human tear fluids are shown in Figure S4. Each DCD-SERS spectrum showed the distinct vibration characteristics of the tear biofluids used. Baseline-corrected DCD-SERS spectra (red line in top panels) are more likely to show clear Raman bands compared to raw DCD-SERS spectra corrupted by baseline wander (black line in top panels). However, even baseline-corrected DCD-SERS spectra might be ineffective for quantitative analysis of tear biofluids, due to differences in Raman intensity. The normalized DCD-SERS spectra (blue line in bottom panels) are better options for quantitative and qualitative analysis for the early detection of adenoviral conjunctivitis through human tear fluids. In addition, the pre-processed DCD-SERS spectra for BSS, with a relatively lower baseline (Figure S5), could also be compared to human biological fluids. Although this baseline correction and normalization enhances the raw Raman signals, previous studies have compared Raman intensity without this correction.

■ Nanostructure of two SERS substrates

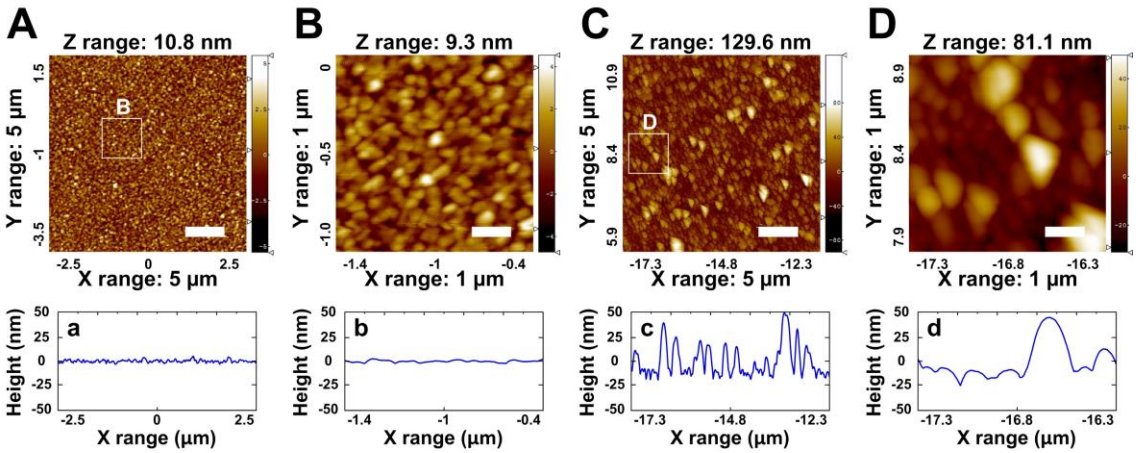

Figure S2. Surface characterization of two gold-coated SERS substrates by AFM. SERS, surface enhanced Raman scattering; AFM, atomic force microscopy. AFM tapping-mode topography with a size of 5 µm×5 µm (A, scale bar=1 µm) and 1 µm×1 µm (B, scale bar=200 nm) for an aluminosilicate substrate coated with 2.5/50 nm Ti/Au (Au.0500.ALSI; Platypus Technologies, Madison, WI, USA). AFM tapping-mode topography with a size of 5 µm×5 µm (C, scale bar=1 µm) and 1 µm×1 µm (D, scale bar=200 nm) for an AAO-based nanodot array substrate coated with 50 nm Au.[10] AAO, anodized aluminum oxide. Line profilers ('a' to 'd') of each substrate clearly showed the surface characteristics of each gold-coated SERS substrate. All AFM tapping-mode topographical images were

obtained using an NANOS N8 NEOS (Bruker, Herzogenrath, Germany) equipped with a 42.5×42.5×4 μm^3 XYZ scanner and two Zeiss optical microscopes (Epiplan 200×/500×). The surface of each SERS substrate was scanned in air with a size of 5×5 μm^2 and a scan speed of 0.8 lines/sec. AFM tapping-mode imaging was performed with 35% relative humidity at room temperature using a silicon cantilever with an integral pyramidal shaped tip (SICONG; Santa Clara, CA, USA). The nominal tip radius and height were <10 nm and 12–16 μm, respectively.

■ Roughness analysis for two SERS substrates

Table S2. Surface roughness of Au.0500.ALSI substrate and AAO nanodot array substrate.*

Surface roughness parameter	Au.0500.ALSI		AAO nanodot array	
Coating	2.5 nm Ti & 50 nm Au		50 nm Au	
EF (10^6)[13]	11.9–12.1		21.6–27.8	
Substrate	Aluminosilicate		AAO-based nanodot array	
Surface roughness parameter	5 μm×5 μm	1 μm×1 μm	5 μm×5 μm	1 μm×1 μm
Mean roughness (nm)	1.0±0.3	0.9±0.2	10.8±2.3	11.9±0.9
RMS roughness (nm)	1.2±0.3	1.1±0.2	14.4±3.7	15.4±1.2
Peak-to-peak height roughness (nm)	10.8±1.1	9.3±0.8	129.6±12.6	81.1±7.5

*AAO, anodized aluminum oxide; EF, enhancement factor; RMS, root-mean-square.

■ Activity of two SERS substrates using BSS solution

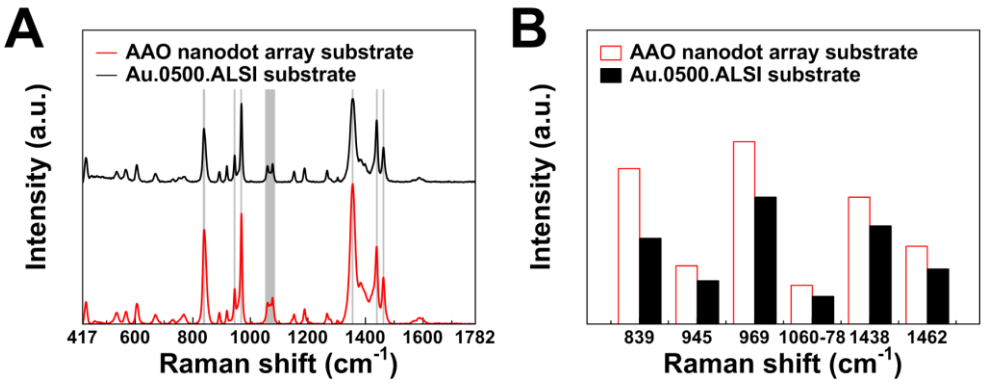

Figure S3. Representative SERS responses of BSS sterile irrigating solution with two SERS substrates. BSS, balanced salt solution (pH 7.5, 300 mOsm/kg; Alcon Laboratories Inc., Fort Worth, TX, USA). (A) All DCD-SERS spectra and (B) prominent Raman bands at 839, 945, 969, 1060–1078, 1356, 1438, and 1462 cm^{-1}. These spectra were measured in the center and were not normalized. DCD-SERS, drop-coating deposition surface enhanced Raman scattering.

■ Pre-processing of DCD-SERS spectra for human tear fluids

Since all DCD-SERS measurements were performed in different environments with different conditions, the intensity

and shape of corrupted baseline wander varied. Therefore, all raw DCD-SERS spectra were first averaged using MATLAB computing software (MathWorks Inc., Natick, MA, USA) to assess signal-to-noise spectral quality and then baseline corrected using a concave rubberband algorithm, which performed ten-iterations on 64-point to aid in preliminary evaluation and peak assignment.[14–16] Without applying an additional smoothing algorithm, the resulting DCD-SERS spectra were normalized by setting the variance of the Raman spectral signal to a value of 1.0, the intense peak was at 1003 cm^{-1} (the ring breath of phenylalanine). The DCD-SERS experimental setup for tear fluids was optimized to overcome a limit in the amount of human tear fluids that could be collected and their low concentration.

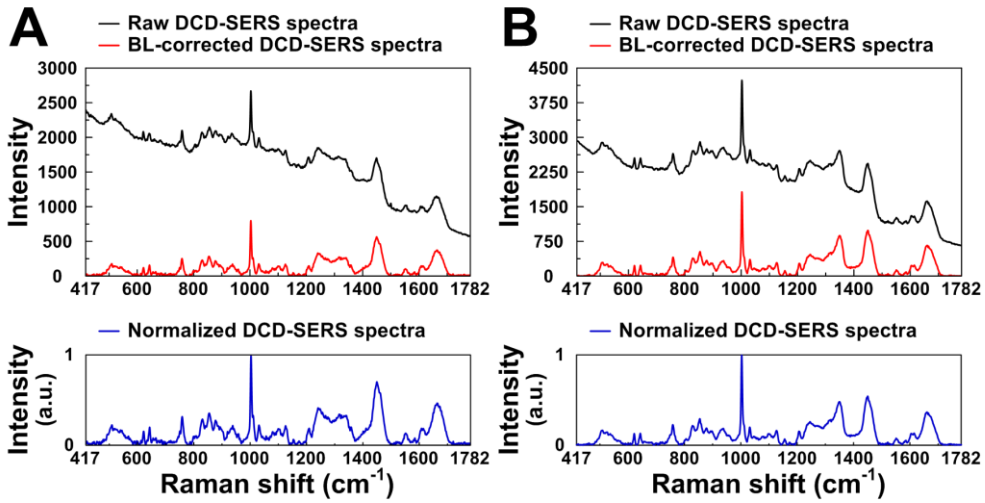

Figure S4. Preprocessing procedure of representative DCD-SERS spectra for (A) normal tear fluids and (B) adenoviral conjunctivitis-diseased tear fluids. BL, baseline. Both DCD-SERS spectra were acquired in the central zone of a dried teardrop.

■ Pre-processing of DCD-SERS spectra for BSS solution

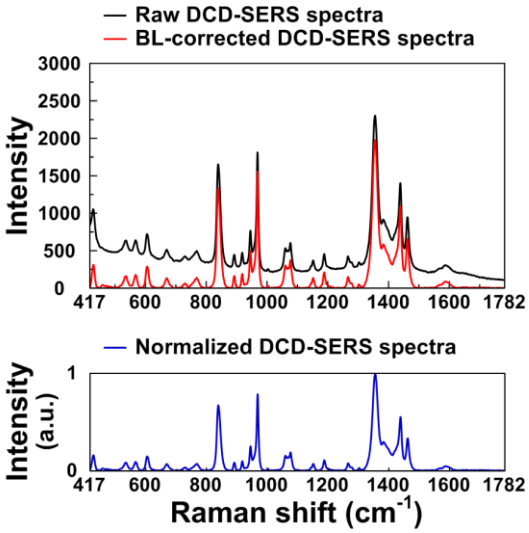

Figure S5. Preprocessing procedure of representative DCD-SERS spectra for BSS.

■ Intensity of DCD-SERS spectral signals with teardrop volumes

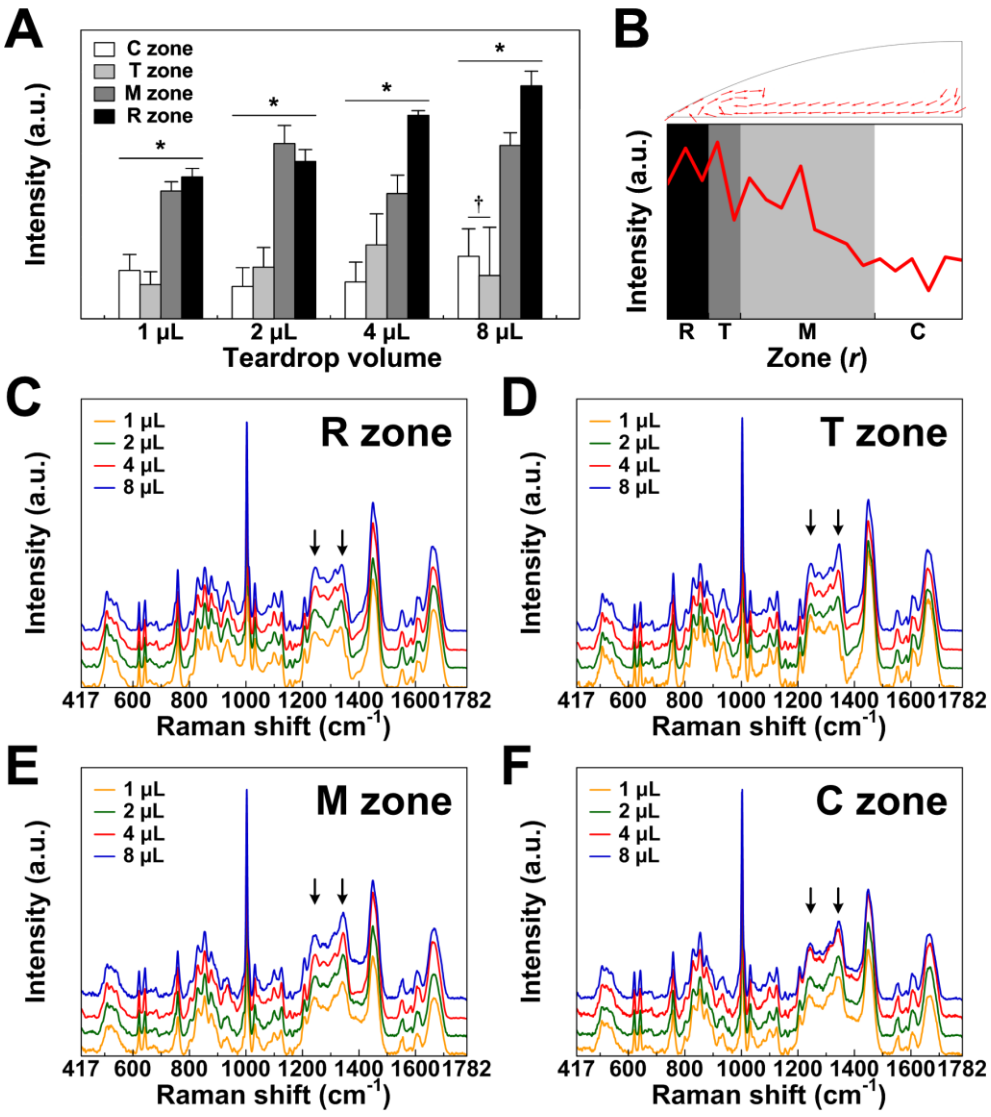

Figure S6. Intensity of DCD-SERS spectral signals of a dried teardrop with adenoviral conjunctivitis according to zone and initial teardrop volume. (A) Comparison of DCD-SERS spectral intensities across zones with teardrop volumes of 1 to 8 μL. *, P<0.001 (ANOVA test) with a *post-hoc* SNK test of P<0.05; †, insignificance (a *post-hoc* SNK test of P>0.05). (B) Finite element modeling of liquid flows in an evaporating tear droplet on an unheated SERS substrate, performed with COMSOL Multiphysics 4.1 (COMSOL Inc., Burlington, MA, USA; Figure S6, Supporting Information). Line profile of the intensity of DCD-SERS spectral signals in each region of a dried teardrop. Representative DCD-SERS spectral signals after the normalization procedure with the tear droplet volumes in the R zone (C), T zone (D), M zone (E), and C zone (F). Arrows represent the region of interest (ROI) peaks proposed for diagnosing adenoviral conjunctivitis.

■ Computational modeling of coffee ring by particle movement during evaporation

The two-dimensional model was constructed with finite-element analysis software COMSOL Multiphysics 4.1

(COMSOL Inc., Burlington, MA, USA). A structured mesh with approximately 6,770 triangular elements was generated in the entire fluid model. The no-slip velocity condition at solid boundaries was applied to all the walls. A 500-particle was released at the center point (0, 0) with initial velocity components of zero. The transmission probability from the inner to the outer zone was computed by counting the number of particles in the outer zone and dividing by the total number of particles. Figure S7 shows the plot of the particle movements over time during evaporation of a teardrop.

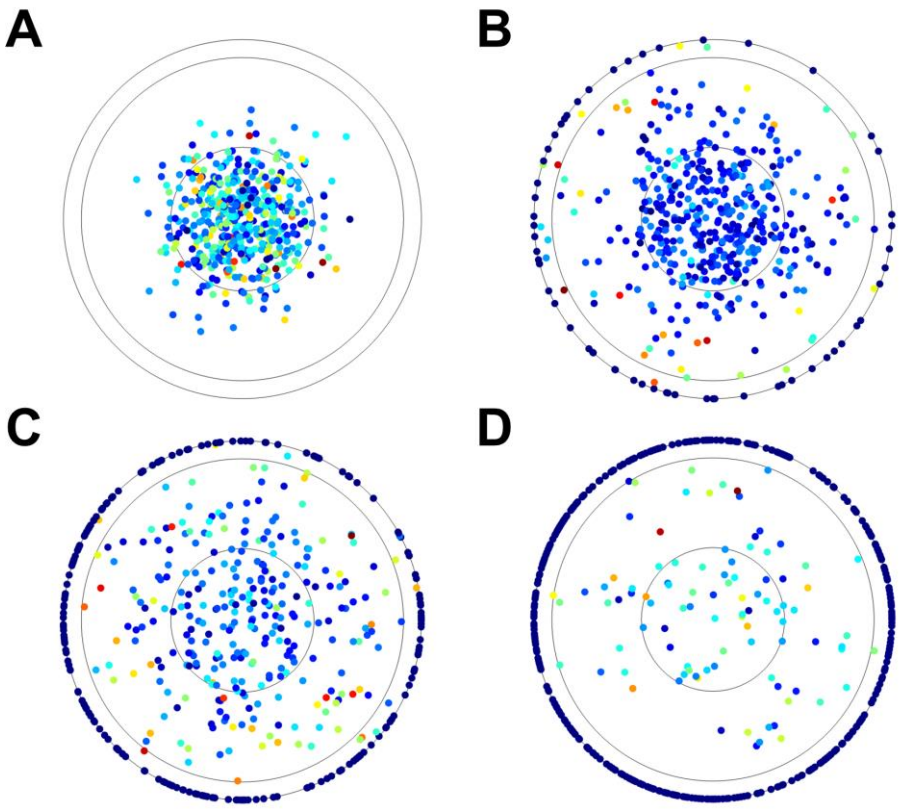

Figure S7. Computational fluidic modeling of particle movements after t sec (A), 2·t sec (B), 3·t sec (C), and 4·t sec (D) during evaporation of tear fluids.

■ Uniformity and reproducibility of DCD-SERS spectra

In order to validate the reliability of DCD-SERS spectra, DCD-SERS spectra were measured randomly from ten different positions in multiple zones of a dried 2-μL tear. The mean pairwise linear correlation coefficient of ten DCD-SERS spectra was 99.29±0.04% (CORR function in MATLAB computing software) as shown in Figure S8. The mean intensity of the spot-to-spot variations in the DCD-SERS peaks at 1242 and 1342 cm^{-1} was 340.68±26.47 and 275.88±20.2, respectively. Their coefficients of variation were <8% (7.77% at 1242 cm^{-1} and 7.37% at 1342 cm^{-1}). In fact, the intensity of the DCD-SERS signals was controlled by DCD effects, SERS effects, laser source focusing,

biosamples, and several other variables. Although the Raman intensity varied among detection sites, the overall variance below 8% affirms the high reproducibility of the DCD-SERS method. Therefore, the noise-independence, uniformity and reproducibility of DCD-SERS spectral signals suggest that the proposed DCD-SERS assessment has the potential to be used as a highly sensitive and selective assessment for tear biofluids. In addition, in order to investigate the considerable stability of DCD-SERS spectra in the ambient environment, DCD-SERS spectra of both groups were collected over a period of time (14 weeks). Measurement longer after evaporation led to neither a significant change in DCD-SERS intensity nor a shift in the prominent DCD-SERS peaks (not show).

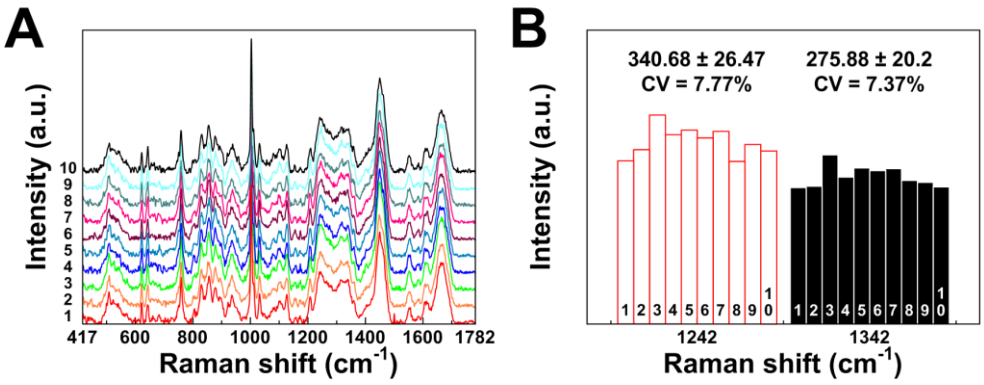

Figure S8. (A) Uniform DCD-SERS spectra obtained from ten different positions for normal human tear fluids and (B) reproducible DCD-SERS spectra in two ROI Raman peaks at 1242 and 1342 cm^{-1}. CV, coefficient of variation; ROI, region of interest. The mean intensity of DCD-SERS spectra in two ROI Raman peaks at 1242 and 1342 cm^{-1} was 340.68 and 275.88 (before normalization), respectively, and the CVs of DCD-SERS spectra in each peak were less than 8%.

■ Inspection of DCD-SERS spectra for tear biofluids

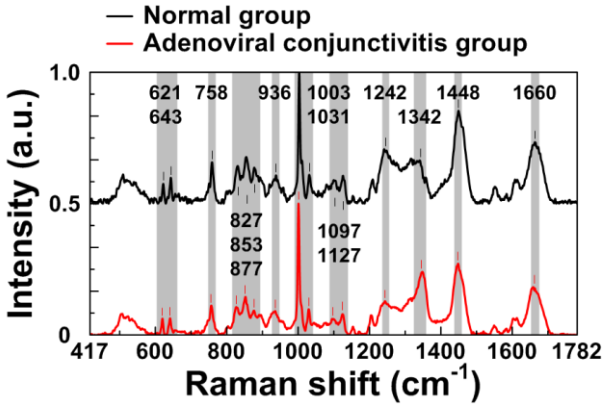

Figure S9. Representative DCD-SERS spectra and prominent peak assignments for normal and adenoviral conjunctivitis-infected human tear fluids. Both DCD-SERS spectra were acquired in the central zone.

Figure S9 shows the typical DCD-SERS spectra of normal and adenovirus-infected tear biofluids. Each DCD-SERS peak showed the distinct vibration characteristics of human tear fluids. Both groups showed intense peaks at 621 cm^{-1} (5-member ring deformation), 643 cm^{-1} (thymine ring angle bend), 758 cm^{-1} (tryptophan ring breath), 827 cm^{-1} (tryosine out of plane ring breath), 853 cm^{-1} (tryosine ring breath), 877 cm^{-1} (symmetric C–C stretching in lipids), 936 cm^{-1} (C–C backbone in proteins), 1003 cm^{-1} (phenylalanine symmetric ring breath), 1031 cm^{-1} (phenylalanine), 1097 cm^{-1} (O–P–O stretching), 1127 cm^{-1} (C–N and C–C stretching in proteins), 1242 cm^{-1} (amide III β-sheet), 1275 cm^{-1} (amide III α-helix), 1342 cm^{-1} (C–H deformation in proteins), 1448 cm^{-1} (C–H deformation in DNA/RNA, proteins, lipids and carbohydrates), and 1660 cm^{-1} (amide I α-helix). There was no shift of these DCD-SERS peaks between normal and infected tears. However, as briefly-mentioned previously, the DCD-SERS intensity of two prominent peaks at 1242 and 1342 cm^{-1} varied between the normal and infected tears. Thus, the intensity ratio of the amide III β-sheet at 1242 cm^{-1} to the C–H deformation at 1342 cm^{-1} could be used as a marker to detect adenoviral conjunctivitis (refer to Eq. (1)). Figure S9 shows the normalized DCD-SERS intensities for healthy and infected tears. The normal tears showed intensities of 0.4084 for 1242 cm^{-1} peak, 0.3232 for the 1342 cm^{-1} peak and 0.6897 for the 1448 cm^{-1} (basal) peak while the tears infected with adenovirus showed an intensity of 0.2418 at 1242 cm^{-1}, 0.4815 at 1342 cm^{-1} and 0.5281 at 1448 cm^{-1}. The I_{1242}/I_{1342} ratio was 1.26 for the normal tears and 0.50 for the infected tears. This significant difference indicates that the ratio of the peak intensity is an effective signature for detecting adenoviral conjunctivitis. The intensity of the 1448 cm^{-1} peak (C–H deformation vibration) decreased approximately 23% after infection. The detailed interpretation is explained in the multiple Gaussian peaks (MGP) biomarker subsection. Although four papers have previously reported tear fluid analysis using Raman spectroscopy, there have been no reports regarding Raman peak assignments. Previous studies used Raman waveforms of PCs to discriminate between the two groups. This method is unsuitable for clinical application due to the performance degradation incurred from the need for many calculations and the memory these calculations require.

■ Diagnostic test

In this study, five parameters (sensitivity, specificity, accuracy, error rate, and prevalence) were calculated using the following equations;

$$\text{Sensitivity} = \frac{\text{TP}}{\text{TP} + \text{FN}}, \tag{S5}$$

$$\text{Sensitivity} = \frac{\text{TN}}{\text{TN} + \text{FP}}, \tag{S6}$$

$$\text{Accuracy} = \frac{\text{TP} + \text{TN}}{\text{TP} + \text{FP} + \text{TN} + \text{FN}}, \tag{S7}$$

$$\text{Error rate} = \frac{FP + FN}{TP + FP + TN + FN}, \quad \text{(S8)}$$

$$\text{Prevalence} = \frac{TP + FN}{TP + FP + TN + FN}, \quad \text{(S9)}$$

where TP denotes true positive, TN denotes true negative, FP denotes false positive, and FN denotes false negative.

Table S3. Performance of logarithmic AC biomarker for normal and adenoviral conjunctivitis-infected human tear fluids (Table S4).

Measure	Normal group				Adenoviral conjunctivitis group			
	C zone	M zone	T zone	R zone	C zone	M zone	T zone	R zone
Sensitivity (%)	100	100	100	100				
Specificity (%)					100	100	100	100
Accuracy (%)	100	96	95	94	100	98	79	60
Error rate (%)	0	4	5	6	0	2	21	40
Prevalence (%)	100	96	95	94	0	2	21	40

*C, central zone; M, middle zone; T, secondary ring zone (an intermediate layer of ring); R, primary ring zone (an outer layer of ring).

Table S4. Outcomes of clinical tests (n=100 for each).

Dried teardrop	Normal group					Adenoviral conjunctivitis group				
	Total	TP	TN	FP	FN	Total	TP	TN	FP	FN
C zone	100	100	0	0	0	100	0	100	0	0
M zone	100	96	0	4	0	100	0	98	0	2
T zone	100	95	0	5	0	100	0	78	0	21
R zone	100	94	0	6	0	100	0	60	0	40

Table S5. Performance of logarithmic AC biomarker according to adenoviral conjunctivitis severity (Table S6).

Measure	Mild adenoviral conjunctivitis group				Severe adenoviral conjunctivitis group			
	C zone	M zone	T zone	R zone	C zone	M zone	T zone	R zone
Specificity (%)	100	100	100	100	100	100	100	100
Accuracy (%)	100	96	80	27	100	100	78	86
Error rate (%)	0	4	20	73	0	0	22	14

Table S6. Outcomes of clinical tests separated by adenoviral conjunctivitis severity (n=50 for each).

Dried teardrop	Mild adenoviral conjunctivitis group					Severe adenoviral conjunctivitis group				
	Total	TP	TN	FP	FN	Total	TP	TN	FP	FN
C zone	50	0	50	0	0	50	0	50	0	0
M zone	50	0	48	0	2	50	0	50	0	0
T zone	50	0	40	0	10	50	0	39	0	11
R zone	50	0	12	0	33	50	0	43	0	7

Table S7. AUC analysis of PCA biomarkers in each zone of a dried teardrop.

PCA biomarker	C zone	M zone	T zone	R zone
[1242, 1342] cm^{-1}	0.9427	0.9007	0.8790	0.7577
[1242, 1448] cm^{-1}	0.9260	0.8767	0.8423	0.7517
[1342, 1448] cm^{-1}	0.9673	0.9707	0.9550	0.9453

Table S8. Performance of PCA biomarkers in each zone of a dried teardrop.

PCA biomarker	Sensitivity (%)				Specificity (%)			
	C zone	M zone	T zone	R zone	C zone	M zone	T zone	R zone
[1242, 1342] cm^{-1}	100.0	93.3	100.0	95.0	89.2	86.6	81.6	70.0
[1242, 1448] cm^{-1}	86.6	91.6	93.3	100.0	97.7	86.6	81.6	65.0
[1342, 1448] cm^{-1}	93.3	95.0	98.3	98.3	96.6	98.3	95.0	91.6

Table S9. Characteristic features of multiple Gaussian peaks for normal and adenovirus-infected tear fluids in each zone of a dried teardrop.

C-zone of a dried teardrop				
m-Gaussian peak	Normal group			
	Area	Intensity	Raman shift (cm^{-1})	Half-width (cm^{-1})
P1	2.69 ± 1.63	0.1655 ± 0.0457	1205.72 ± 0.98	14.69 ± 6.61
P2	4.41 ± 1.09	0.1314 ± 0.0187	1241.37 ± 3.51	12.49 ± 2.45
P3	23.30 ± 8.22	0.2487 ± 0.1647	1274.79 ± 4.34	72.01 ± 14.19
P4	18.66 ± 2.91	0.4221 ± 0.0526	1315.81 ± 4.31	42.32 ± 11.04
P5	7.24 ± 5.65	0.2709 ± 0.1395	1340.59 ± 1.48	23.01 ± 6.44
P6	6.66 ± 5.89	0.2682 ± 0.2197	1358.15 ± 2.41	21.37 ± 7.34
P7	6.05 ± 4.02	0.1798 ± 0.0906	1390.72 ± 8.56	28.56 ± 9.23
P8	4.83 ± 5.59	0.1574 ± 0.1192	1413.25 ± 7.93	22.93 ± 11.87
P9	2.60 ± 3.24	0.1516 ± 0.1480	1426.91 ± 13.89	12.77 ± 5.49
P10	27.13 ± 1.61	0.7355 ± 0.1020	1453.86 ± 5.01	34.99 ± 3.96
m-Gaussian peak	Adenoviral conjunctivitis group			
	Area	Intensity	Raman shift (cm^{-1})	Half-width (cm^{-1})
P1	3.87 ± 2.66	0.1550 ± 0.0522	1206.77 ± 1.52	21.31 ± 8.92
P2	13.78 ± 2.57	0.3251 ± 0.0704	1242.77 ± 1.73	40.63 ± 8.61
P3	6.50 ± 3.63	0.2063 ± 0.1001	1276.80 ± 1.31	28.37 ± 4.27
P4	12.32 ± 2.41	0.3295 ± 0.0925	1310.49 ± 1.06	36.02 ± 6.09
P5	11.70 ± 1.71	0.3831 ± 0.0697	1342.40 ± 3.17	28.97 ± 3.42
P6	2.83 ± 2.20	0.1449 ± 0.1020	1358.97 ± 0.75	16.11 ± 4.39
P7	5.62 ± 1.00	0.1888 ± 0.0511	1382.61 ± 1.79	28.73 ± 4.94
P8	3.09 ± 1.32	0.1489 ± 0.0690	1403.84 ± 2.77	19.78 ± 2.07
P9	2.00 ± 1.37	0.1154 ± 0.0644	1418.43 ± 1.01	15.15 ± 2.91
P10	24.29 ± 4.64	0.6077 ± 0.1292	1450.99 ± 0.92	37.66 ± 0.84

M-zone of a dried teardrop				
m-Gaussian peak	Normal group			
	Area	Intensity	Raman shift (cm^{-1})	Half-width (cm^{-1})
P1	1.59 ± 0.21	0.1435 ± 0.0133	1206.56 ± 0.06	10.41 ± 0.70
P2	5.36 ± 1.39	0.1918 ± 0.0307	1239.60 ± 0.74	25.94 ± 2.56
P3	21.07 ± 2.63	0.2831 ± 0.0090	1275.77 ± 0.50	69.85 ± 7.94
P4	6.97 ± 1.19	0.2105 ± 0.0321	1317.84 ± 0.71	31.09 ± 1.55
P5	4.61 ± 1.49	0.2051 ± 0.0554	1341.04 ± 0.50	20.81 ± 1.59
P6	2.49 ± 2.12	0.1128 ± 0.0123	1355.91 ± 9.08	21.10 ± 18.81
P7	1.27 ± 0.77	0.0559 ± 0.0137	1374.84 ± 11.30	22.85 ± 15.07
P8	3.05 ± 0.61	0.1222 ± 0.0145	1403.58 ± 2.11	23.30 ± 2.15
P9	0.77 ± 0.14	0.0621 ± 0.0058	1418.93 ± 0.93	11.58 ± 1.67
P10	24.86 ± 0.46	0.6298 ± 0.0096	1451.74 ± 0.11	37.09 ± 0.80
m-Gaussian peak	Adenoviral conjunctivitis group			
	Area	Intensity	Raman shift (cm^{-1})	Half-width (cm^{-1})
P1	1.98 ± 1.45	0.1260 ± 0.0494	1205.69 ± 0.79	14.26 ± 7.57
P2	10.74 ± 4.54	0.2595 ± 0.0994	1241.89 ± 1.92	39.28 ± 13.90
P3	5.01 ± 2.93	0.1555 ± 0.0762	1274.86 ± 3.08	28.73 ± 9.87
P4	13.60 ± 6.66	0.2672 ± 0.1021	1313.51 ± 3.49	46.74 ± 18.54
P5	6.69 ± 4.78	0.2319 ± 0.1356	1342.72 ± 2.91	24.91 ± 9.53
P6	1.66 ± 1.65	0.0826 ± 0.0658	1358.46 ± 1.06	15.17 ± 8.31
P7	3.97 ± 1.83	0.1262 ± 0.0529	1388.31 ± 5.90	29.26 ± 9.78
P8	1.84 ± 0.97	0.0900 ± 0.0411	1407.25 ± 3.44	18.85 ± 6.24
P9	0.82 ± 0.58	0.0638 ± 0.0310	1419.14 ± 1.169	11.35 ± 4.33
P10	21.42 ± 8.14	0.5279 ± 0.2005	1451.31 ± 0.77	38.17 ± 11.54

T-zone of a dried teardrop				
m-Gaussian peak	Normal group			
	Area	Intensity	Raman shift (cm^{-1})	Half-width (cm^{-1})
P1	1.43 ± 0.02	0.1205 ± 0.0004	1206.56 ± 0.02	11.17 ± 0.08
P2	8.56 ± 0.10	0.2559 ± 0.0018	1240.34 ± 0.06	31.41 ± 0.16
P3	8.84 ± 0.08	0.2137 ± 0.0005	1273.96 ± 0.05	38.85 ± 0.26
P4	9.38 ± 0.17	0.2385 ± 0.0015	1315.67 ± 0.20	36.97 ± 0.44
P5	4.21 ± 0.13	0.1830 ± 0.0024	1342.26 ± 0.02	21.62 ± 0.39
P6	1.42 ± 0.04	0.0986 ± 0.0020	1360.06 ± 0.06	13.54 ± 0.08
P7	2.56 ± 0.01	0.0720 ± 0.0006	1388.05 ± 0.10	33.39 ± 0.10
P8	2.31 ± 0.00	0.1024 ± 0.0005	1406.82 ± 0.08	21.20 ± 0.06
P9	0.75 ± 0.00	0.0617 ± 0.0000	1419.73 ± 0.08	11.42 ± 0.08
P10	22.11 ± 0.05	0.5482 ± 0.0017	1452.16 ± 0.03	37.89 ± 0.03
m-Gaussian peak	Adenoviral conjunctivitis group			
	Area	Intensity	Raman shift (cm^{-1})	Half-width (cm^{-1})
P1	1.53 ± 0.26	0.1338 ± 0.0108	1206.72 ± 0.51	10.67 ± 1.12
P2	9.08 ± 3.29	0.2666 ± 0.0732	1242.24 ± 1.19	31.18 ± 4.16
P3	11.17 ± 11.05	0.2066 ± 0.0703	1275.36 ± 2.44	44.54 ± 31.31
P4	14.07 ± 8.36	0.2522 ± 0.0816	1314.50 ± 0.48	48.43 ± 21.46
P5	6.34 ± 2.16	0.2417 ± 0.0579	1344.42 ± 3.49	24.15 ± 2.81
P6	0.64 ± 0.42	0.0558 ± 0.0263	1360.42 ± 0.43	10.07 ± 2.15
P7	3.08 ± 1.25	0.0952 ± 0.0236	1390.78 ± 4.46	29.65 ± 4.22
P8	1.27 ± 0.38	0.0673 ± 0.0143	1408.75 ± 1.01	17.58 ± 1.42
P9	0.51 ± 0.08	0.0514 ± 0.0058	1419.87 ± 0.18	9.35 ± 0.46
P10	25.07 ± 1.23	0.6279 ± 0.0339	1452.46 ± 0.61	37.52 ± 0.24

R-zone of a dried teardrop				
m-Gaussian peak	Normal group			
	Area	Intensity	Raman shift (cm^{-1})	Half-width (cm^{-1})
P1	1.61 ± 0.29	0.1286 ± 0.0160	1206.19 ± 0.40	11.71± 0.69
P2	10.00 ± 4.76	0.2659 ± 0.0908	1240.49 ± 1.67	34.07 ± 4.81
P3	7.14 ± 1.90	0.1833 ± 0.0256	1273.59 ± 1.32	36.37 ± 7.58
P4	13.61 ± 4.64	0.2835 ± 0.0465	1316.58 ± 2.03	44.17 ± 8.83
P5	3.76 ± 1.89	0.1693 ± 0.0632	1342.20 ± 1.13	20.12 ± 2.56
P6	2.01 ± 1.41	0.1147 ± 0.0610	1358.89 ± 1.69	15.76 ± 3.19
P7	2.56 ± 0.77	0.0762 ± 0.0182	1390.01 ± 4.29	30.98 ± 3.69
P8	1.60 ± 0.60	0.0771 ± 0.0208	1407.82 ± 1.25	19.07 ± 2.41
P9	0.58 ± 0.18	0.0514 ± 0.0110	1419.51 ± 0.43	10.34 ± 1.21
P10	22.21 ± 3.72	0.5586 ± 0.0899	1451.90 ± 0.62	37.32 ± 0.58
m-Gaussian peak	Adenoviral conjunctivitis group			
	Area	Intensity	Raman shift (cm^{-1})	Half-width (cm^{-1})
P1	1.80 ± 0.39	0.1472 ± 0.0209	1205.93 ± 0.62	11.41 ± 0.95
P2	5.04 ± 1.92	0.1667 ± 0.0510	1237.58 ± 1.90	27.89 ± 2.76
P3	16.46 ± 6.11	0.2353 ± 0.0363	1275.33 ± 0.57	64.44 ± 18.20
P4	7.45 ± 2.52	0.2176 ± 0.0481	1316.50 ± 1.06	31.47 ± 4.35
P5	5.92 ± 1.82	0.2374 ± 0.0424	1340.81 ± 0.89	22.99 ± 3.32
P6	1.18 ± 0.31	0.0878 ± 0.0183	1359.63 ± 0.59	12.50 ± 1.40
P7	2.15 ± 0.63	0.0677 ± 0.0141	1391.77 ± 6.50	30.00 ± 7.24
P8	1.19 ± 0.76	0.0590 ± 0.0235	1409.21 ± 3.64	17.93 ± 4.92
P9	0.55 ± 0.24	0.0522 ± 0.0126	1420.05 ± 0.84	9.64 ± 2.14
P10	21.47 ± 2.23	0.5661 ± 0.0469	1451.19 ± 0.81	35.58 ± 0.93

Table S10. DCD-SERS shift of MGP biomarkers and characteristic features (area and intensity) in each zone of a dried teardrop.

MGP biomarker	Normal group (cm^{-1}) (intensity feature) / (area feature)				Adenoviral conjunctivitis group (cm^{-1}) (intensity feature) / (area feature)			
	C zone	M zone	T zone	R zone	C zone	M zone	T zone	R zone
Amide III β-sheet	1241	1240	1240	1240	1243	1242	1242	1238
	(0.13)	(0.19)	(0.26)	(0.27)	(0.33)	(0.26)	(0.27)	(0.17)
	(4.40)	(5.36)	(8.56)	(10.00)	(13.78)	(10.74)	(9.08)	(5.04)
Amide III α-helix	1275	1276	1274	1274	1277	1275	1275	1275
	(0.25)	(0.28)	(0.21)	(0.18)	(0.21)	(0.16)	(0.21)	(0.24)
	(23.30)	(21.07)	(8.84)	(7.14)	(6.50)	(5.01)	(11.17)	(16.46)
C–H deformation	1341	1341	1342	1342	1342	1343	1344	1341
	(0.27)	(0.21)	(0.18)	(0.17)	(0.38)	(0.23)	(0.24)	(0.24)
	(7.24)	(4.61)	(4.21)	(3.76)	(11.70)	(6.69)	(6.34)	(5.92)
C–H deformation	1454	1452	1452	1452	1451	1451	1452	1451
	(0.74)	(0.63)	(0.55)	(0.56)	(0.61)	(0.53)	(0.63)	(0.57)
	(27.13)	(24.86)	(22.11)	(22.21)	(24.29)	(21.42)	(25.07)	(21.47)

References

(1) Zhang, D.; Xie, Y.; Mrozek, M. F.; Ortiz, C.; Davisson, V. J.; Ben-Amotz, D. *Anal. Chem.* **2003**, *75*, 5703–5709.

(2) Reyes-Goddard, J. M.; Barr, H.; Stone, N. *Photodiagnosis Photodyn. Ther.* **2008**, *5*, 42–49.

(3) Filik, J.; Stone, N. *Anal. Chim. Acta* **2008**, *616*, 177–184.

(4) Filik, J.; Stone, N. *Analyst* **2007**, *132*, 544–550.

(5) Kuo, M. T.; Lin, C. C.; Liu, H. Y.; Chang, H. C. *Invest. Ophthalmol. Vis. Sci.* **2011**, *52*, 4942–4950.

(6) Kuo, M. T.; Lin, C. C.; Liu, H. Y.; Yang, M. Y.; Chang, H. C. *Invest. Ophthalmol. Vis. Sci.* **2012**, *53*, 1436–1444

(7) Abdi, H.; Williams, L. J. *Wiley Interdisciplinary Reviews: Computational Statistics* 2012, 2, 433–459.

(8) Liu, C.; Zheng, D.; Zhao, L.; Liu, C. *Biomed. Mater. Eng.* **2014**, 24, 271–277.

(9) Wang, L.; Xu, L.; Feng, S.; Meng, M. Q.; Wang, K. *Comput. Biol. Med.* **2013**, 43, 1661–1672.

(10) Jung, G. B.; Bae, Y. M.; Lee, Y. J.; Ryu, S. H.; Park, H. K. *Appl. Surf. Sci.* **2013**, *282*, 161–164.

(11) Podstawka**,** E**.;** Sikorska**,** E**.;** Proniewicz**,** L**.** M.; Lammek**,** B. *Biopolymers* **2006,** 83**,** 193–203.

(12) Musumeci, A. W.; Frost, R. L.; Waclawik, E. R. *Spectrochim. Acta A Mol. Biomol. Spectrosc.* **2007**, 67, 649–661.

(13) Smythe, E. J.; Dickey, M. D.; Bao, J.; Whitesides, G. M.; Capasso, F. *Nano Lett.* **2009**, 9, 1132–1138.

(14) Driskell, J. D.; Tripp, R. A. *Chem. Commun.* **2010**, *46*, 3298–3300.

(15) Hennigan, S. L.; Driskell, J. D.; Dluhy, R. A.; Zhao, Y.; Tripp, R. A.; Waites, K. B.; Krause, D. C. *PLoS One* **2010**, *5*, e13633.

(16) Hennigan, S. L.; Driskell, J. D.; Ferguson-Noel, N.; Dluhy, R. A.; Zhao, Y.; Tripp, R. A.; Krause, D. C. *Appl. Environ. Microbiol.* **2012**, *78*, 1930–1935.